Available online at www.sciencedirect.com

ScienceDirect

journal homepage: www.elsevier.com/locate/he

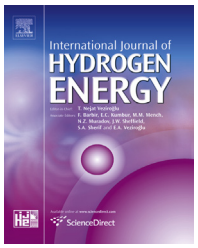

Waveform characteristics and losses of a new double sided axial and radial flux generator

Halil Gor [a,*], Erol Kurt [b]

[a] Hakkari University, Faculty of Engineering, Department of Electrical and Electronics Engineering, 30000 Hakkari, Turkey

[b] Gazi University, Faculty of Technology, Department of Electrical and Electronics Engineering, 06500 Teknikokullar, Ankara, Turkey

ARTICLE INFO

Article history:
Received 30 November 2015
Received in revised form
27 December 2015
Accepted 27 December 2015
Available online 19 January 2016

Keywords:
Double sided
Generator
Loss
Waveform
THD

ABSTRACT

In this paper, the waveform characteristics and the losses of a new three phase permanent magnet generator, which has a rated power 250 W at 1000 rpm have been explored theoretically and experimentally. The proposed generator has new flux morphology with the axial and radial directions, therefore the waveform characteristics become important for this new machine. The detailed phase voltage measurements prove that the machine generates sinusoidal waveform and the total harmonic distortion (THD) is found to be sufficient for such a new prototype machine. According to the detailed experimental measurements, the machine has THD values of 0.4% and 4.7% for resistive load and no-load cases. In addition, the losses and the efficiency measurements are found to be very promising although the airgap optimization has not been completed. According to the simulation studies, the machine has the core and copper losses of 2.5 W and 23 W for loaded cases, respectively.

Introduction

The motivation on the axial flux permanent magnet generators (AFPMG) enhances due to their compactness, high power densities and natural cooling mechanisms [1]. The invention of the first axial flux generators went to 150 years before [2]. Indeed, the production of the NdFeB magnets has accelerated the motivation for the design and generation of new permanent magnet (PM) machines from 1980s and this trend still continues due to some advantages of the PM usage [3]. Frankly speaking, PM machines have better power density and cogging torque value, cheaper construction and higher moment values [4]. Besides, the phase waveform can be obtained sinusoidal from the output [5–7]. For instance, although the power densities change from one machine to the other, the machines with power densities from 6 kW/m^3 to 710 kW/m^3 can be encountered in literature [8].

In reality, the geometry and flux topology are the key points to increase the power densities in AFPMG. For instance, Vansompel, et al. [9] explored the effects of core shapes, laminations over the efficiency in an AFPMG by using FEA. In addition, the effect of airgap and the core losses were also investigated by the same group by using the same method in terms of efficiency. It has been known that the core mass and volume should be minimized in the designs since it affects the

* Corresponding author.
E-mail address: halilgor30@hotmail.com (H. Gor).
http://dx.doi.org/10.1016/j.ijhydene.2015.12.172

weight, efficiency and compactness of the machine [10]. In AFPMGs, the stators and rotors can be designed in many combinations. They can be double sided as in our research, or more stators and rotors can be added [11]. The double sided machines become much energetic than the single sided ones due to the coil numbers [12].

The machines can be designed with different core types. They can be designed as slotted or slotless. In most of the designs, the laminated cores are used. While the slotted cores assist to decrease the cogging torque, slotless designs manage to lower the mutual and loss inductances [13]. However one should keep in mind that the magnetic force between the cores and magnets should be optimized in order to decrease the cogging torque [14]. Indeed, the magnetic force causes extreme mechanical stress and vibrations in the machine, the air gaps in axial machines should be larger than those of radial flux ones [12]. The airgap can be designed from 1 mm to 4 mm with respect to the mechanical processing. It should be noted that the airgap affects the entire output of the machine [15]. Thus, the airgap optimization should be performed in a new design [16]. In the coreless machines, the windings should be put into a non-magnetic and insulating material such as epoxy, polyamide, etc. Due to the lack of the cores, there exists no core loss and cogging torque and the machines becomes lighter. However, there can be eddy losses at higher speeds in the windings [16]. On the other hand, the disadvantage of the machine is the low magnetic fluxes Φ compared to the machines with cores and high copper losses. These are the main factors to decrease the efficiency of AFPMGs [17]. The lower airgap values cause higher power (P_{out}) as a result of inducting higher voltages in the windings [18]. Whereas forming a stable airgap between the rotors and stators is hard in the axial machines.

AFPMGs are especially appropriate for medium speed applications; therefore they can be used in robotics, electrical vehicles, trains, etc [19]. In wind energy applications, they are preferred to neglect the gear systems in the turbine. Comparing the axial flux machines with the radial ones, axial flux machines have lower cogging torques and volume and higher power density and efficiency [20]. In addition, the installation of axial flux machines is easier than the radial ones due to the direct addiction to the blades. Jian and colleagues [21] found that the heating of the AFPM machines could be caused by their higher power densities. Therefore, an efficient geometry for the rotors and stators should be designed and the large rotor and stator surfaces of these machines can also help to solve this problem [19]. The air gap is also vital to overcome from this heating problem [2]. However the key point in the design is to determine the appropriate shape of the permanent magnets, since all shapes of the magnets cannot give perfect sinusoidal output. The use of Nd-based magnets has an advantage on the determination of their shapes. Technically, it is possible to produce different shapes of magnets [22]. There can be different types of combinations for the stator and rotor designs. For instance, rotor can be one sided and stators can be double sided or vice versa [10,11]. However, the important point is that the double sided machines can have double energy generation relative to the one sided ones [23].

In this study, we report the recent analyses on the losses and the harmonic analyses of the new AFPMG. Design of Generator section gives a brief explanation on the design and specifications of new machine. Theoretical background on basic connection of phases and losses are given in Theoretical background Section. Experimental Section represents the experimental details of the generator. The main findings on the experiments and simulations are reported in the next section. Finally, the paper ends with the concluding remarks on the findings of the study.

Design of generator

In this work, the design and implementation of an axial/radial flux PM generator with three phases are reported. Initially the designed machine is depicted in Fig. 1. The machine has double rotors at the upper and lower parts and a stator is situated between these rotors. The stator has three main units in order to provide a stable machine especially at high rotations.

The rotors are connected to each other and rotate at two sides on the same shaft. The design has a specific laminated core structure and it has been proven in Ref. [22] that this structure gives lower cogging torque values. Note that the small laminated cores have certain advantages on the machine weight and eddy currents. Since the cores are slotless, they are easy to produce, technically.

The windings, magnets and cores have circular shapes. Since the machine is a three phase one, the design consists of 16 magnets and 12 windings and cores. Note that two windings sit on each core (Fig. 2). In the design, an air gap of 5 mm is used. Due to many air gaps inside the stator unit and air gaps between the rotor and stator, the design has an efficient natural cooling mechanism on the large rotor and stator surface.

The B–H curve of the core material is presented in Fig. 3. The core material has high flux density value up to 1.5 T, which is already sufficient for our application. In the entire FEA simulations, this curve is used for the core characterization.

Each core has 40 laminated layers with the thickness of 0.5 mm each. Note that 40 layers are combined together in axial direction, thus the flux loss is minimized in the axial direction. The coils are positioned as in Fig. 2. In order to decrease the copper losses, circular shape windings are preferred in the design as mentioned in Ref. [23]. Another design advantage is that the windings on the circular shapes can be produced easily than the trapezoidal or triangular ones. The magnets are located symmetrically near the upper and lower ends of the cores in N–S–N–S orientation with opposite

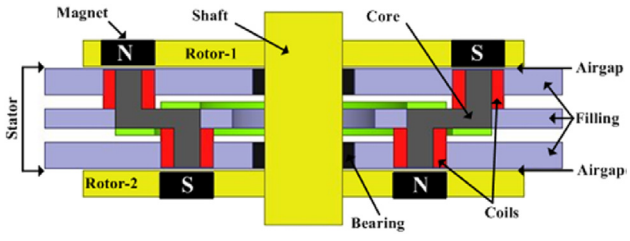

Fig. 1 – A new AFPMG design and units.

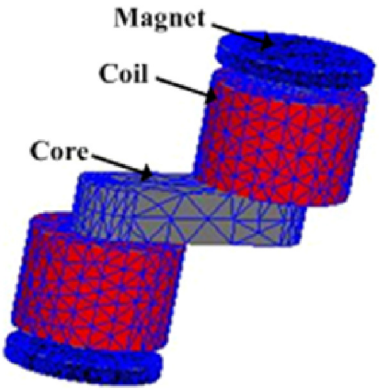

Fig. 2 – The specific core structure and windings at both ends with the meshes.

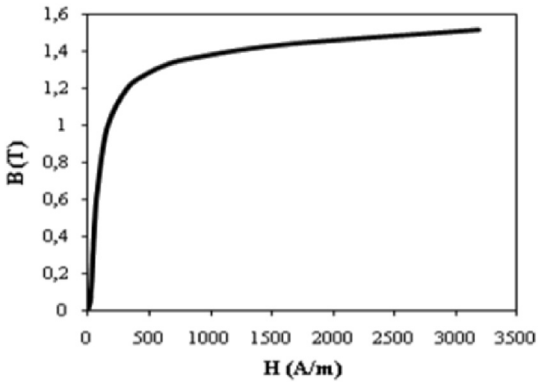

Fig. 3 – *B*–*H* curve of M530 – 50A stainless steel.

poles. Between the magnets, the electrical angle is adjusted to 30° in the simulations.

The combination of windings should be realized in such a way that no phase shift cannot be produced from one winding to other. In addition, upper and lower windings should be put into the same connection as in Fig. 4.

The flux lines are shown in Fig. 5, when the generator operates. Since the machine is three phase, the core and magnet numbers differ. Indeed, some cores have high fluxes such as the first, the fourth, the seventh and the tenth cores from left to right, others have lower ones for a certain time.

The flux pattern forms closed lines among the magnets, when the directions of magnets are positioned at the same directions of cores for four windings as a result of three phase formation. These maximal fluxes disappear, when the electrical angle changes due to the rotation. Therefore an additional reluctance occurs for different electrical angles due to 16 magnets and 12 cores.

Theoretical background

The designed generator has both axial and radial directed flux and it differs from the other axial machines in that context. The radial directed flux assists to decrease the cogging torque. The equivalent circuit is summarized in Fig. 6.

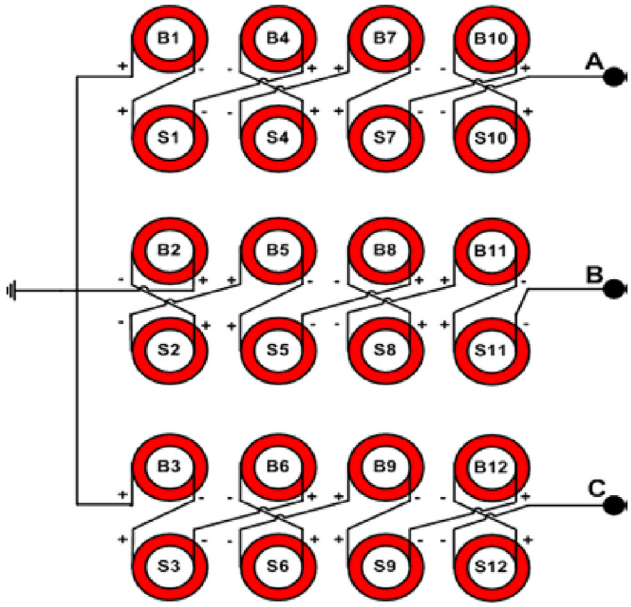

Fig. 4 – The connections of individual windings. B(S) is used for upper(lower) windings of corresponding core.

According to three phase construction, the serial connected windings are classified to three different clusters. Note that each phase includes the windings situated at small and large diameters in order to form identical output waveforms. The net voltage of each phase is the sum of the generated voltage of each winding. In that case, the total inductance of one phase can be written as,

$$L_{pA} = L_{B1} + L_{S1} + L_{B4} + L_{S4} + L_{B7} + L_{S7} + L_{B10} + L_{S10} \quad (1)$$

Considering the net voltage drop on the load and windings, one arrives at,

$$v_{LpA} - v_{RA} - v_{LA} = 0 \quad (2)$$

If the voltage expressions are written explicitly,

$$\frac{di_A}{dt} = \frac{i_A}{L_{pA}}(R_A + R_{LA}) \quad (3)$$

is obtained. Here, I is the generated current in the windings for each phase. On the other hand, the induced voltage on a phase can be written as,

$$v_{LpA}(t) = -8N\frac{d\phi(t)}{dt} \quad (4)$$

Here, the factor 8 denotes the winding numbers in single phase and N shows the winding turn. Thus, the generated instantaneous power from three phases can be written as,

$$P_{out} = 3\, v(t)\, i(t) \quad (5)$$

if $v(t)$ and $i(t)$ are considered for single phase and the power factor is set to 1.

In general, the losses of a generator occur as copper losses, core losses and mechanical losses [13,19]. Since the losses strictly depend on the input and output powers, one calculates the losses related with the output power as follows:

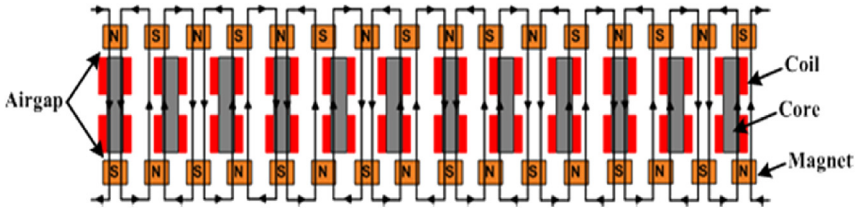

Fig. 5 – Magnetic flux lines representation in the single phase machine.

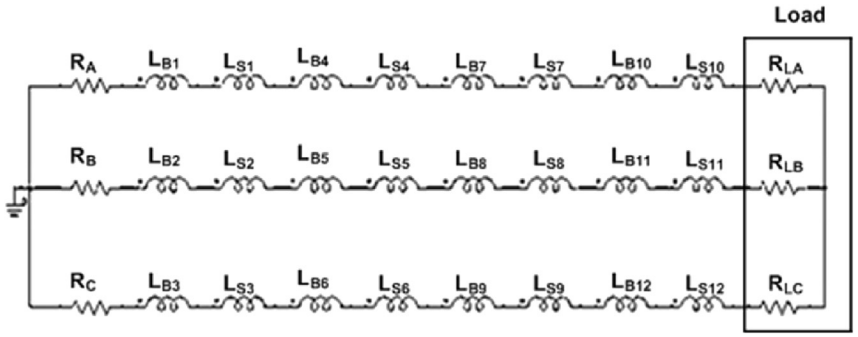

Fig. 6 – The equivalent circuit of the proposed machine.

$$P_{out} = m\, v(t)\, i(t) \tag{6}$$

Here m, $v(t)$ and $i(t)$ denote the phase number, phase voltage and current at the instantaneous time. Within this notation, copper losses can be written as follows:

$$P_{cu} = m\, i(t)^2\, R_p \tag{7}$$

Eq. (7) is another form of Eq. (6). Since Joule heating occurs in the windings, it can be represented by current $i(t)$ flowing inside the windings. Note that phase resistance is denoted by R_p. Stator is responsible for this losses due to the fact that all windings are positioned inside stator. Core losses can be negligible for the permanent magnets, since it is at the low order. For the other part of the machine, these losses are given by W/kg in terms of material type and feature. In general, core losses consist of three losses, namely hysteresis, eddy and anomalous losses [24]. In this manner, they can be summarized as follows:

$$P_{Fe} = P_h + P_e + P_a \tag{8}$$

$$P_h = k_h \frac{f}{50} B_{pk}^{1.8} W_{fe} \tag{9}$$

$$P_e = k_e \left(\frac{f}{50} B_{pk}\right)^2 W_{fe} \tag{10}$$

$$P_a = k_a \left(\frac{f}{50} B_{pk}\right)^{1.5} W_{fe} \tag{11}$$

Here P_e, P_{Fe}, P_h, P_a, W_{Fe}, B_{pk}, k_a, k_e and k_h represent eddy, core, hysteresis and anomalous losses (in W), core mass, peak value of flux density (in T), coefficients of anomalous loss, eddy loss and hysteresis loss. In the light of formulation above, the efficiency can be calculated as follows [24]:

$$\eta = \frac{P_{out}}{P_{out} + \Delta P} \times 100 \tag{12}$$

Here ΔP denotes the total losses of the machine.

Experimental

Fig. 7 presents the prototype machine. Three different colors (in web version) indicate three phase connections. On the same shaft, two rotors made by Aluminum can freely rotate.

In order to avoid the mechanical frictions, 5 mm airgap has been adjusted in that prototype machine, whereas the optimized airgap can be obtained after the cogging torque and waveform measurements. Fig. 7 is a slotless drum-typed wired double sided and cored machine. At the middle, the stator is kept fixed and the rotors can rotate due to two bearings. The design features of the machine have been presented by Table 1.

As stated in the previous section, double sided machines are better for power densities than the single side ones. In addition, the double sided machines have better mechanical balance since it has two moving parts at each side. Besides, the double air gap opportunity of the machine in two sides of stator can help to decrease the heat especially produced at high rotation speeds. All these advantages can give a chance to load the machine with high resistive electrical loads [25]. The construction of the machine is easy since the windings can be obtained easily and put into the tips of the core. In order to decrease the structural cost and the copper losses, lower winding numbers are preferred, whereas extremely low winding numbers lower the power generation [26]. The present machine uses the drum-type circular winding, since this type winding has certain advantages to lower the copper

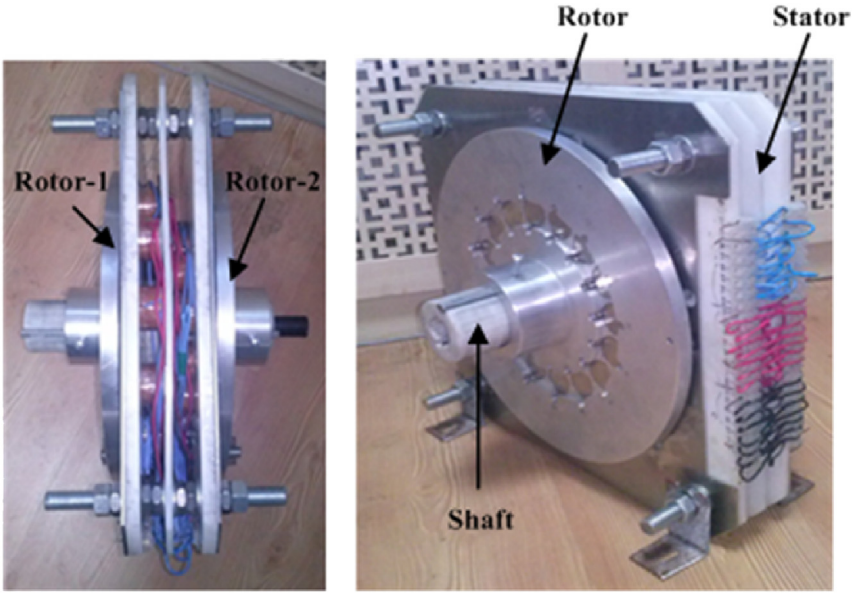

Fig. 7 – The front and side view of the designed and constructed machine.

Table 1 – Design parameters of the proposed generator.

Components	Features
Inner radius of rotor R_2 (mm)	75
Outer radius of rotor R_2 (mm)	105
Inner radius of rotor R_1 (mm)	120
Outer radius of rotor R_1 (mm)	150
Inner radius of stator disc (mm)	70
Outer radius of stator disc (mm)	155
Coil inner diameter (mm)	30
Coil outer diameter (mm)	40
Phase	3
Winding turns	200
Coil number	24
Wire diameter (mm)	0.75
Magnet type	NdFeB
Magnet shape	Circular
Magnet number	16
Magnet diameter (mm)	30
Magnet thickness (mm)	5
Core material	M19
Core type	Axially/radially laminated
Core number	12
Air gap (mm)	5
Core coefficients (W/m^3)	
K_h	164.2
K_c	1.3
K_e	1.72
K_{dc}	0

losses [23]. In order to get benefit from the coil active surfaces, the diameters of the magnets and coils should be close to each other.

Fig. 8 presents a core with two windings at the tips. The cores are made by laminated core material given in Table 1. While the upper tip of the core stays at the one side of stator, other situates at the other start side. In the stator, there exist 12 individual cores and the machine has 24 windings.

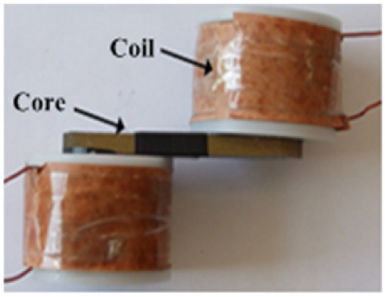

Fig. 8 – A representative core and windings.

In the coreless machines, there exists no cogging torque since they do not include any ferromagnetic material, thereby these kinds of machines can move better at lower speeds. This also causes no hysteresis losses. On the other hand, these machines have high eddy losses due to the lack of flux orientation inside the windings [27]. Therefore the flux density becomes lower at the air gap and that causes to have much lower power generation. Considering the above explanations, the core losses become lower compared to the copper losses in the cored machines, whereas the copper losses become higher in the coreless machines [27,28]. In addition, the laminated core structure also helps to decrease the core losses [9]. In the prototype machine, we have used 40 core layers with 0.5 mm thickness. Due to the original shape of core design, the flux is directed in radial and axial directions. Fig. 9 shows the core tips at two sides of stator.

In one of our previous studies [22], the superiority of the radial/axial directed proposed core structure was reported. It has lower cogging torque value compared to the linear bar shaped core. This result mainly stems from the lower mechanical torque value due to the smaller diameter in one side of the stator, since the torque depends on the magnetic force and the distance of this force to the axis.

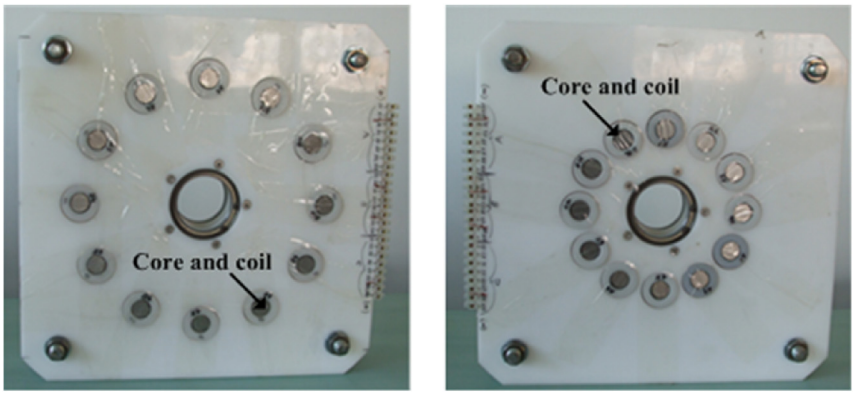

Fig. 9 – The appearance of stator from two sides.

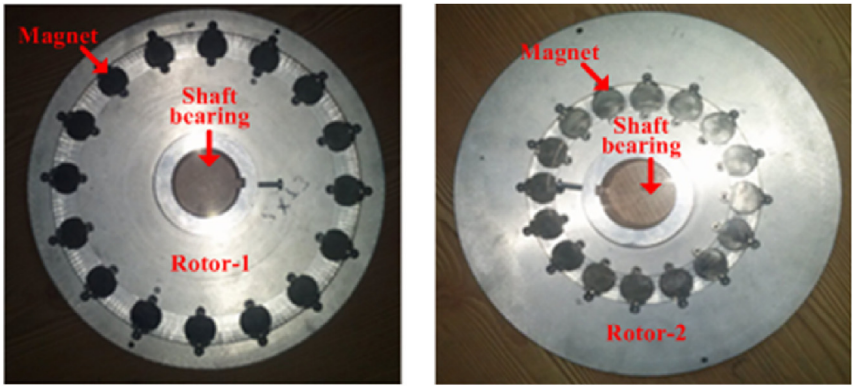

Fig. 10 – Rotor units.

The rotors of new generator are shown in Fig. 10. While one series of magnets are located at the maximal diameter, the other series of magnets are positioned on the smaller diameter. They are structured in disc form. The magnets are made by rare earth material with high magnetic flux density.

Total 32 magnets with the dimensions of 30×5 mm are positioned on the rotors. This orientation has the electrical angle of 22.5° between each magnet.

Results and discussion

Electromagnetic simulations of fluxes and waveforms

In this part, the magnetic flux characteristics are presented for the no-load operation. All simulations have been made by a commercial code which uses the finite element method (FEM) in a magnetodynamics process. Fig. 11 shows a representative plot of the fluxes which are produced for three phases. This result has been obtained at 1000 rpm. A clear symmetry is seen in the waveforms with the appropriate phase shifts in order to produce the three phase effect.

It is obvious that the fluxes are obtained as sinusoidal waveforms, since the disc-type magnets rotate in a circular trajectory. These fluxes induce the phase voltages as given by Fig. 12(a,b) for corresponding rotor speeds. The voltage waveforms are similar to each other at 300 rpm and 1000 rpm for the no-load case. Only the amplitude and frequency increases as usual. The amplitude of each phase is obtained with the phase shift of 120°. At this speed (i.e. 300 rpm), the maximal peak to peak voltage is found as $V_{pp} = 84$ V.

When the rotor speed is increased to 1000 rpm, the maximal peak to peak voltage is found as $V_{pp} = 280$ V. The waveforms are sinusoidal and the phase shift is still preserved perfectly for the three phases. The detailed simulations have proven that the generated voltage increases linearly with the rotor speed as in the literature upto the studied speeds [6,7,22,28,29].

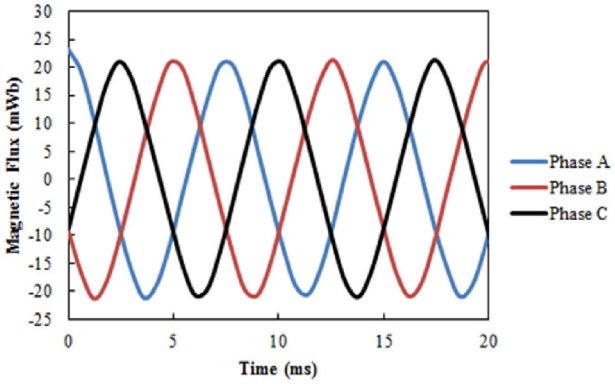

Fig. 11 – Magnetic fluxes of phases at 1000 rpm.

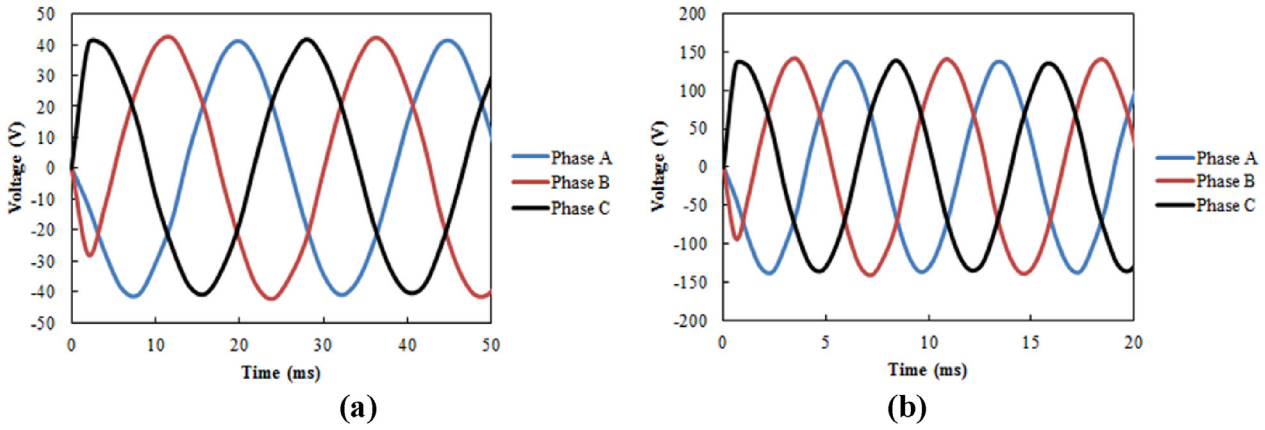

Fig. 12 – No-load output voltage waveform at the rotor speed (a) 300 rpm and (b) 1000 rpm.

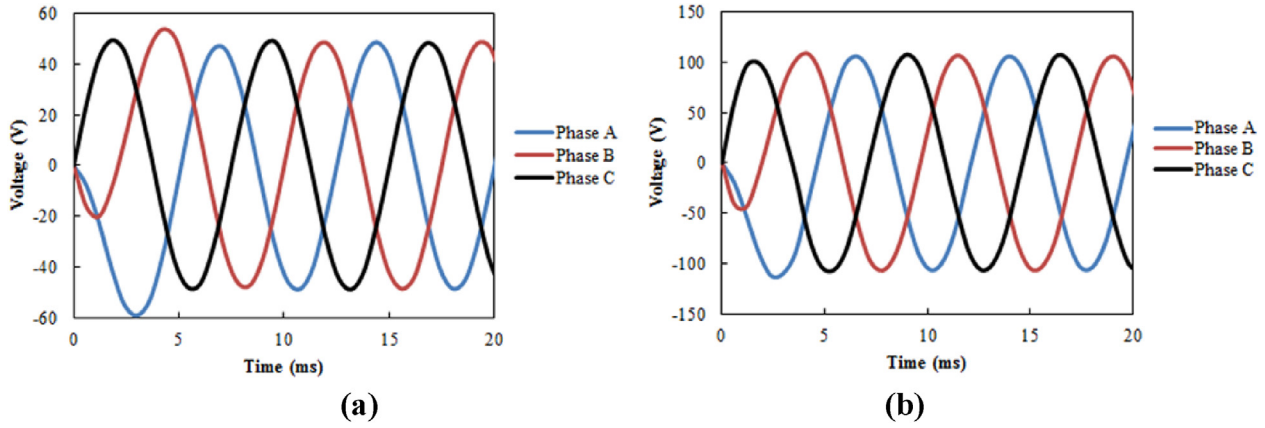

Fig. 13 – The amplitudes at 1000 rpm for the electrical loads of (a) 10 Ω and (b) 40 Ω.

In Fig. 13, the output voltages on two representative resistive loads are shown. The speed is adjusted as 1000 rpm and the electrical load is added to the phases as 10 Ω and 40 Ω. The resistive load causes changes in the amplitudes as usual and a comprehensive study has been performed for the electrical loads for this reason.

The currents flowing through the phases are plotted in Fig. 14. The maximal currents are simulated as $I = 4.47$ A and $I = 2.71$ A over the ohmic loads 10 Ω and 40 Ω at 1000 rpm, respectively.

These current amounts are sufficient for the wires to carry and also the phase shifts are observed very well.

Electromagnetic simulations of cogging torque

The simulations on the cogging torque values are given in this subsection. In order to produce the cogging torque values for different electrical angles, the magnetostatic solutions have been obtained for every 1 ° of rotation. A sample cogging torque plot is presented in Fig. 15.

The cogging torque occurs when the magnets pass nearby the tips of the cores due to the increase of the magnetic force. This effect tries to rotate the machine in the reverse direction and produces a counterpart towards the forward motion of the machine. Indeed, the cogging torque is defined by the reluctance variation in the angular direction of the rotor as given by,

$$T_{cog} = -\frac{1}{2}\emptyset_g^2 \frac{dR}{d\theta} \tag{13}$$

Here Φ_g is the airgap flux, Θ is the rotor angle and R is the airgap reluctance. Since the machine works as 3 phase, the magnetic force cycles for every 7.5°. In the proposed generator, the maximal amount was calculated as 500 mNm, which is fairly low value for this energy scaled machine. According to our earlier theoretical analyzes [22], the phase number of a machine also affects the maximal cogging torque values. Strictly speaking, in a single phase machine the torque values increase substantially compared to the three phase machines since all the core tips get maximal magnetic force synchronously. If both results are compared, a 3-phase generator has certain advantages over the single one, since the angles of magnets differs with the cores substantially. Thus this geometry helps to reduce the cogging torque values in three-phase machines.

Electromagnetic simulations of losses

Fig. 16 shows the core loss at 1000 rpm rotor speed. Note that this data has been simulated for no-load case, thereby it can

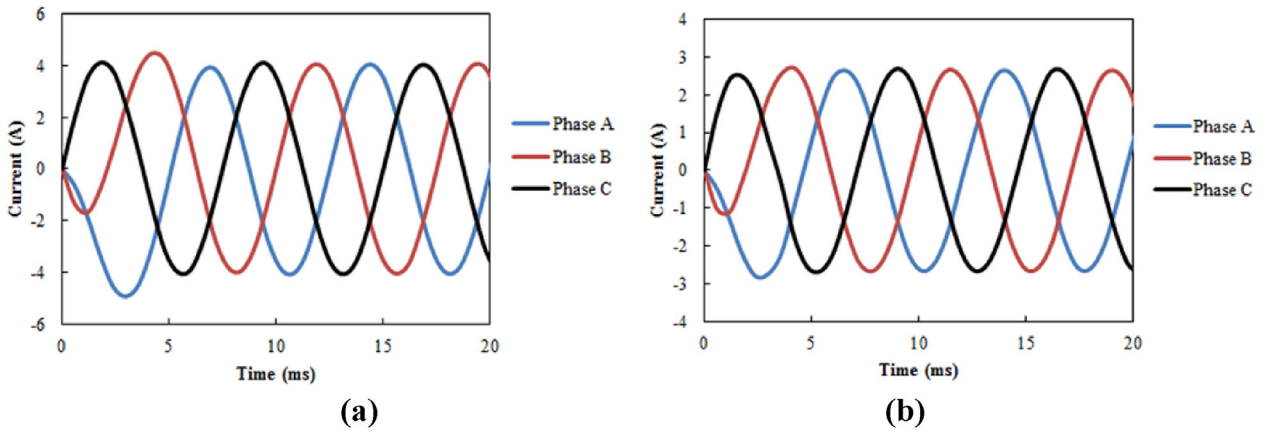

Fig. 14 – Current waveforms over the resistive loads (a) 10 Ω and (b) 40 Ω at 1000 rpm.

be stated that the current flowing the windings should be higher. According to detailed simulations, the core loss has been 0.45 W at the rotor speed of 300 rpm. However Fig. 16 proves that the core loss increases up to 2.5 W for the speed of 1000 rpm. Frankly speaking, the increase in rotor speed causes high change in magnetic flux. Thus, this change yields to higher losses in cores. This situation is also obvious from Eq. (9).

Since there exists no-load, the Copper loss vanishes in that case. However, a certain core loss exists due to the hysteresis and eddy terms. The core loss stays at 2.5 W, which is very low as in Fig. 16.

In the case of 30 Ω electrical load, the losses are given in Fig. 17 for 1000 rpm rotor speed. The core loss value is around 2.5 W, whereas the Copper loss increases up to 23 W due to the electrical load.

This increase in Copper loss stem from the winding current. This result can be seen well in Fig. 18.

When the load current increases the linear increase in Copper loss can be seen clearly from Fig. 18. However, the core loss does not change too much; indeed it slightly decreases for increasing current. According to these plots the resistive load current $I = 2.85$ A produces a Copper loss of 45 W.

In Fig. 19, the core losses at various rotor speeds are plotted. The reported rotor speeds are 300 rpm, 500 rpm and 1000 rpm.

As an overall trend, the rotor speed enhances the core losses. When the speed is 300 rpm, the losses are around 0.6 W, whereas it increases to 2 W at 1000 rpm. The trends of the plots are also different with respect to load. At lower speeds, the cores are almost constant with respect to electrical load. Whereas it increases up to 30 Ω linearly in the case of 1000 rpm, then it becomes constant beyond this load value. If a comparison is made for 40 Ω, the core losses are 0.7 W, 1.2 W and 2.4 W for 300 rpm, 500 rpm and 1000 rpm.

In Fig. 20, Copper losses are shown with respect to resistive load for various rotor speeds. As the general trends of the plots, the increase in load causes a decrease in Copper loss. For instance, at 300 rpm, the Copper loss changes from 11 W to 3 W. Similarly, at 500 rpm, the Copper loss decreases from 23 W to 7 W. In the case of 1000 rpm, the Copper loss decreases from 47 W to 18 W. Thus it is understood that the low load values increases the current flowing through the windings and it causes an enhancement in loss. Therefore, in order to decrease the losses an optimal load value should be adjusted at the output terminals.

The total losses are given in Fig. 21 for various speeds. Since the core losses are very low compared to the Copper losses, the total losses show the trend of Copper losses as in Fig. 20.

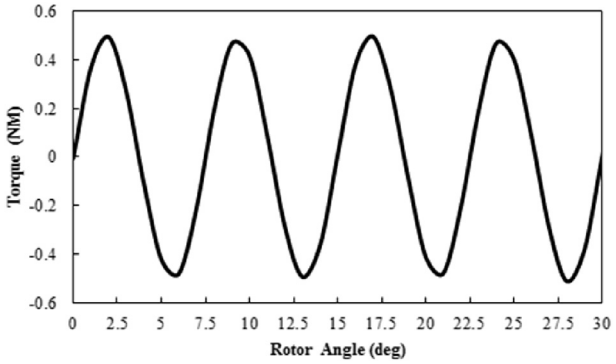

Fig. 15 – The cogging torque values vs. electrical angle.

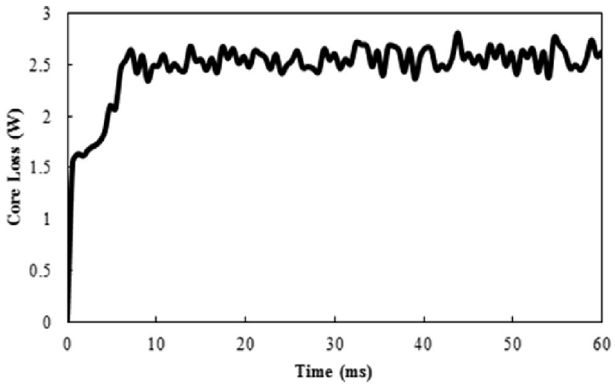

Fig. 16 – Core loss at 1000 rpm rotor speed in the no-load case.

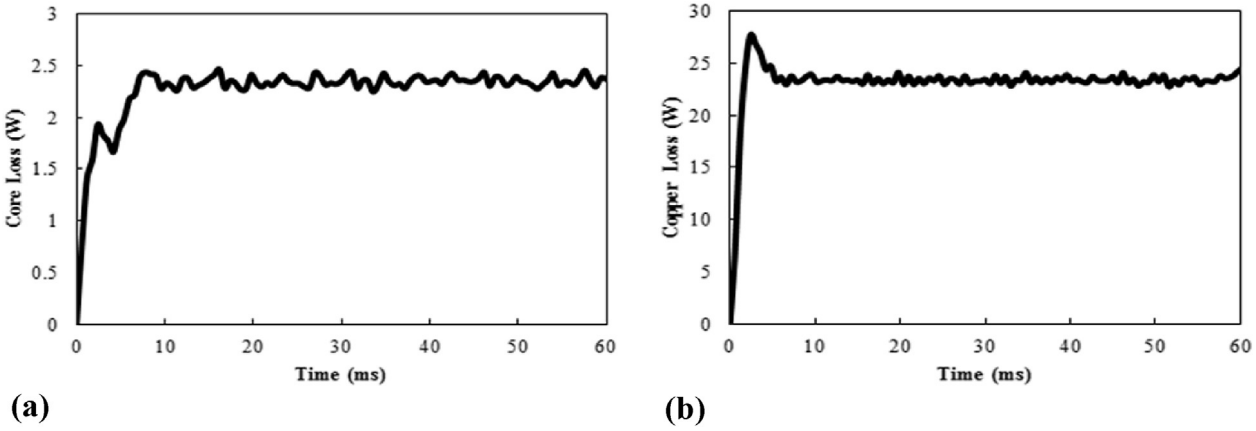

Fig. 17 – (a) Core loss and (b) Copper loss in the case of 30 Ω electrical load. The rotor speed is 1000 rpm.

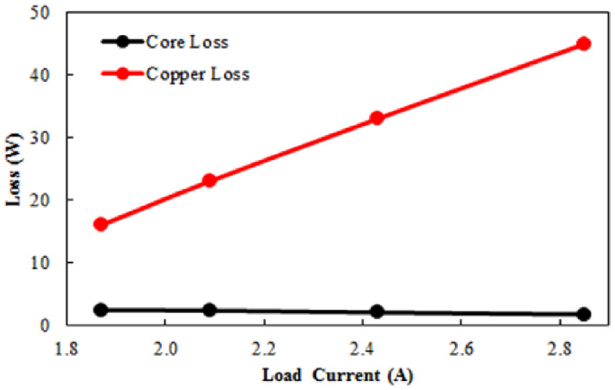

Fig. 18 – Load current with respect to losses.

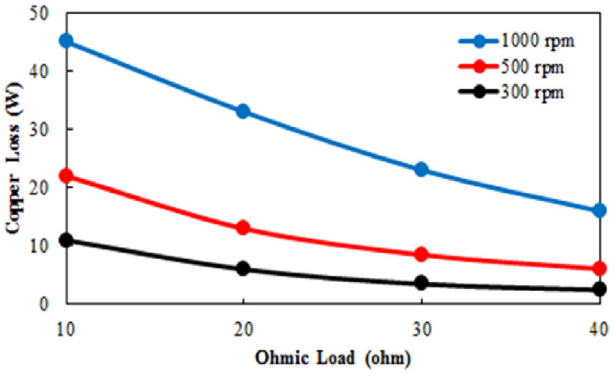

Fig. 20 – Copper loss variations with respect to resistive load in the cases of 300 rpm, 500 rpm and 1000 rpm.

When the rotor speed increases the total loss of the generator increases, but the main criteria for lower losses is that the load should be high enough to set the losses minimal for the machine.

Experimental results of the proposed machine

The setup for the laboratory tests is shown in Fig. 22. The experimental unit basically includes a controller unit which enables us to adjust the rotor speed, an induction motor which drives the proposed AFPMG, coupling units for the AFPMG and electrical loads.

In no-load operation, a representative clear sinusoidal waveform is presented in Fig. 23. The output is obtained as $V_{rms} = 87.8$ V for each phase. This value has been measured at 1000 rpm and gives 120 ° of phase shift as expected.

At 1000 rpm, the sinusoidal waveform gives the value of $V_{rms} = 87.8$ V from each phases. According to detailed THD measurements, there is no important harmonics in the output

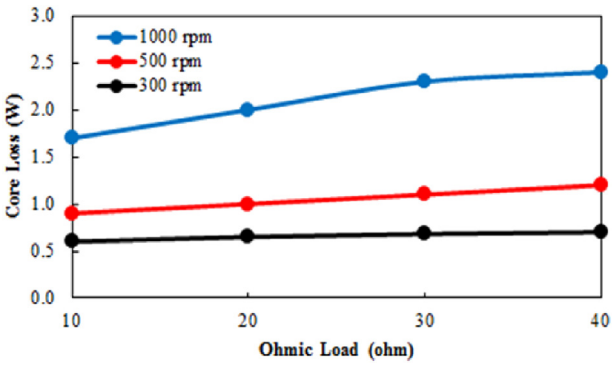

Fig. 19 – The variation of core loss with respect to resistive load in the cases of 300 rpm, 500 rpm and 1000 rpm.

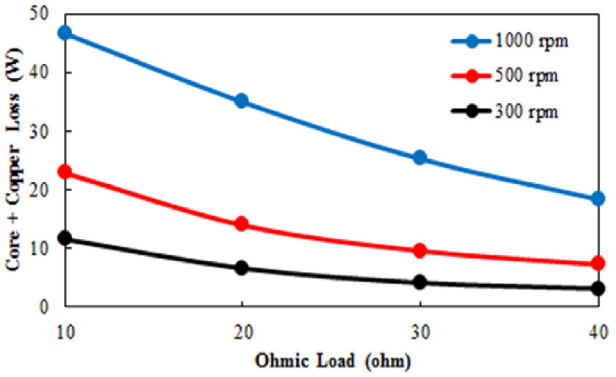

Fig. 21 – The total losses with respect to resistive load for the speeds of 300 rpm, 500 rpm and 1000 rpm.

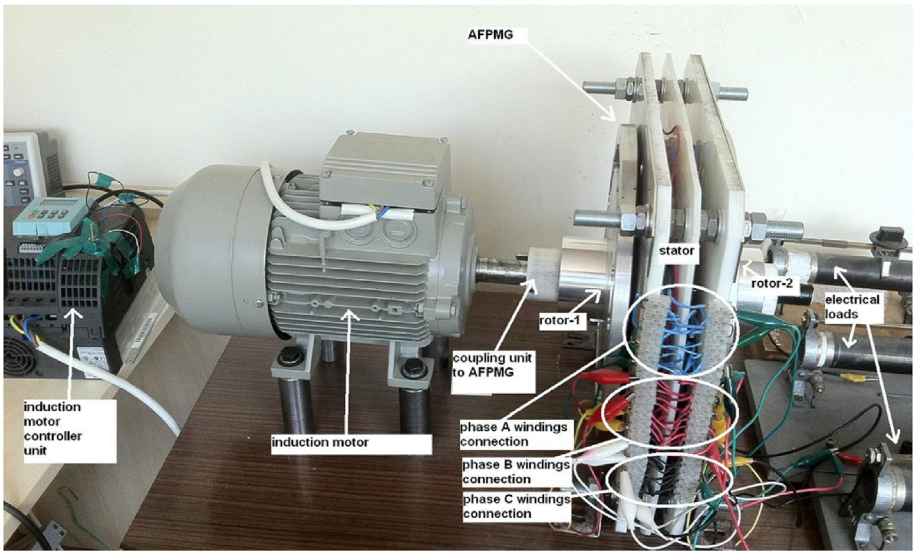

Fig. 22 – The setup for the measurement of the proposed AFPMG.

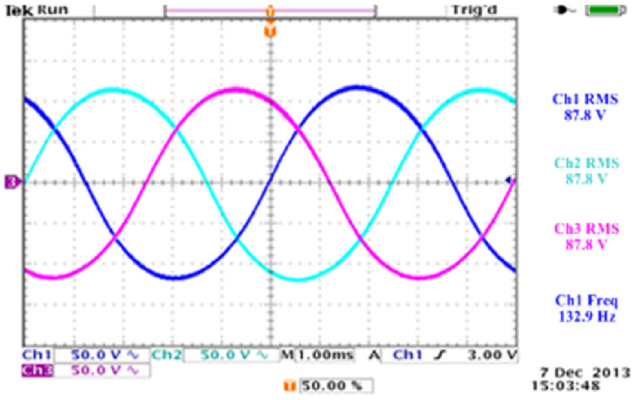

Fig. 23 – No-load output waveforms of three phases of AFPMG at the rotor speed of 1000 rpm.

at this speed. Fig. 24(a,b) give the phase voltages for the electrical loads of 10 Ω and 40 Ω. It is obvious that while the effective value is $V_{rms} = 24.07$ V for $R_L = 10$ Ω, it is increased to $V_{rms} = 57.8$ V for $R_L = 40$ Ω. Thus, this also indicates that the simulations and experiments give the similar character to identify the optimal load conditions.

The harmonic analyses of the waveforms are given in Fig. 25(a–d) for load and no-load cases. In no-load cases, the THD values have been measured as 4.7% for 300 rpm and 1000 rpm. In that case, it has been proven that the machine stability is very well and the waveform characteristics do not change with respect to speed.

Note that the load connection to the output of the machine decreases the harmonics substantially and makes much stable waveform (see in Fig. 25(c,d)). Strictly speaking, the THD values decrease to 0.4% from 4.7%, when 30 Ω load is attached. In the case of no-load case (see in Fig. 25(a,b)) only the third harmonic survives.

A much detailed findings from the THD analyses are given in Fig. 26. From this figure, it is obvious that the electrical load lowers the harmonicity of the machine, significantly.

However, the THD values are nearly fixed for finite loads from 5 Ω to 30 Ω. Thus it is proven that the machine gives a very stable output signal in terms of harmonics. The THD values are measured around 0.4% for all resistive loads at

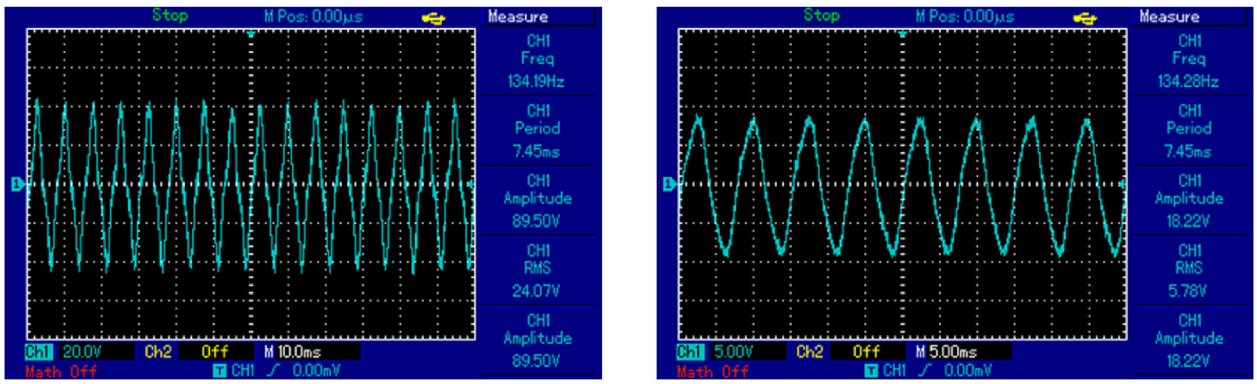

Fig. 24 – Voltage waveforms with resistive loads (a) 10 Ω and (b) 40 Ω at 1000 rpm (the probe is scaled to ×10).

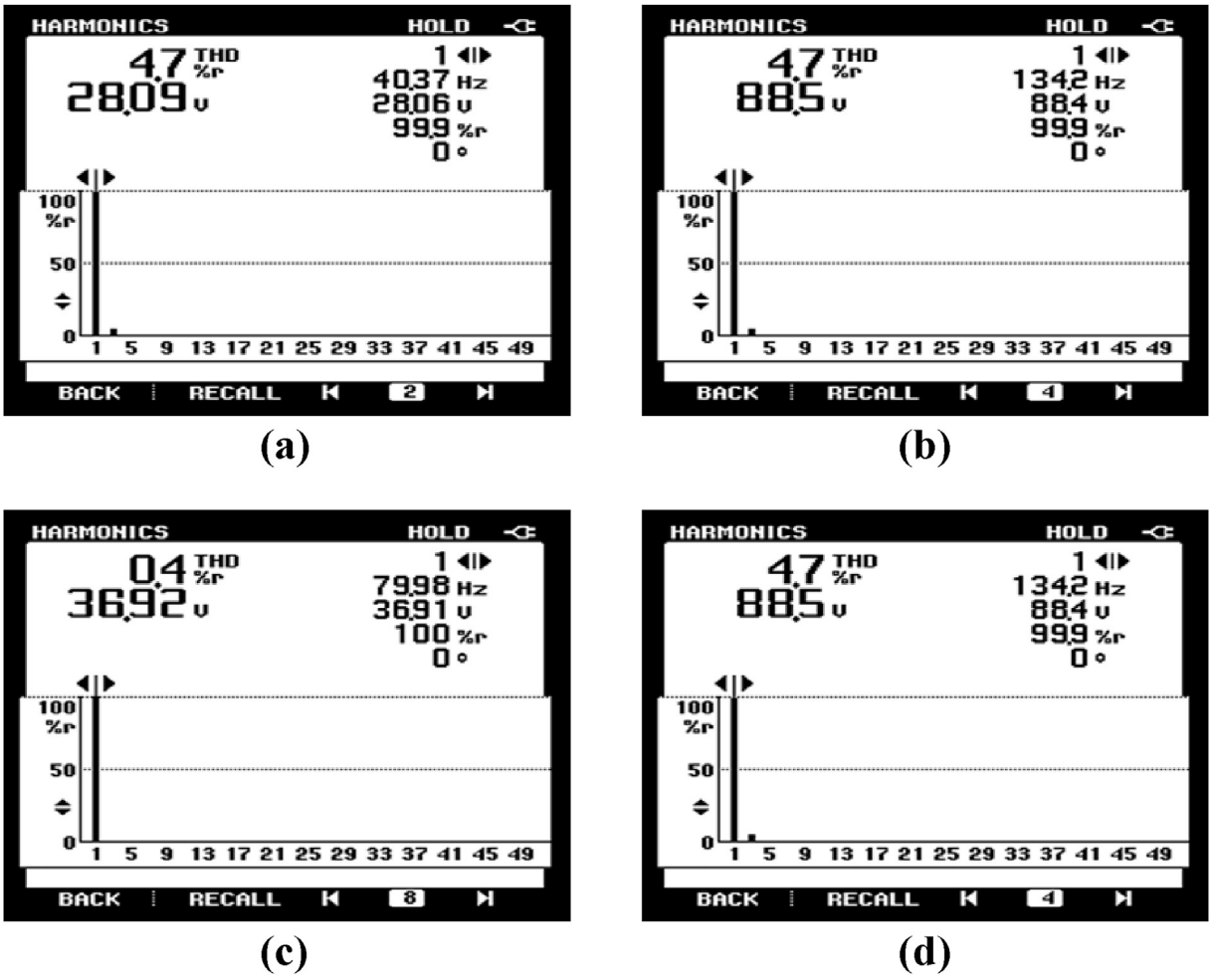

Fig. 25 – The THD values at the speed of (a) 300 rpm and (b) 1000 rpm in the no-load case. The THD values at the speed of (c) 600 rpm and (d) 1000 rpm in the case of 30 Ω load.

increasing speeds. According to some test results, 0.2% THD has also been measured for some load values at various speeds.

The power plots of the proposed machine are given in Fig. 27 for many rotation speeds. With increasing speed, the generated power increases substantially. There exist the general shifting characteristics of the maximum power points with increasing speed.

Indeed, the maximum power points shift to higher resistive loads for increasing load. For instance, the maximum

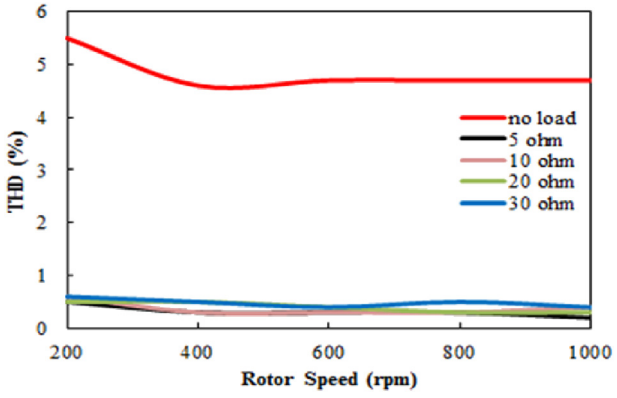

Fig. 26 – THD values from experiments for various load cases.

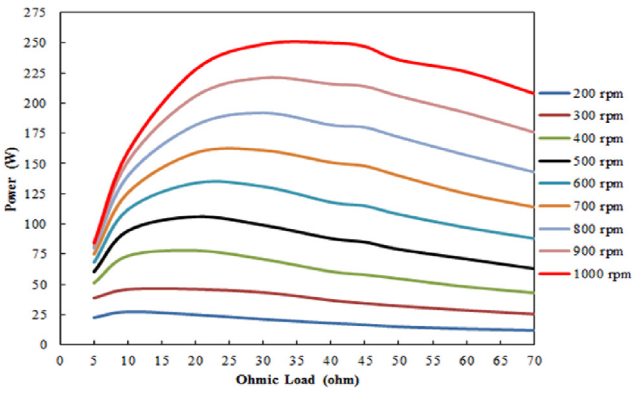

Fig. 27 – Output power via electrical load at different speeds.

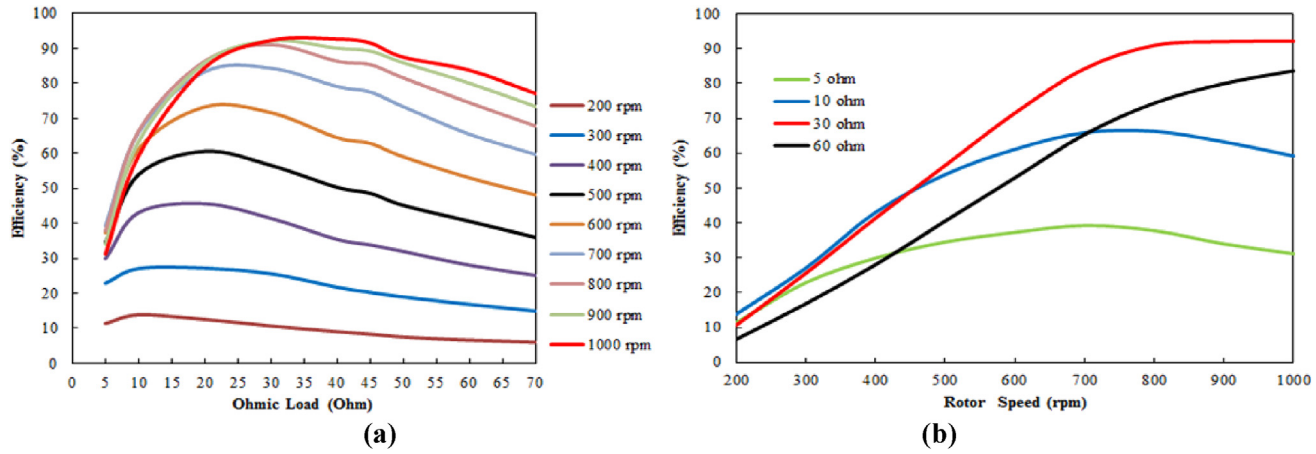

Fig. 28 – Efficiency measurements with respect to (a) electrical load and (b) rotor speed.

power is obtained at 8 Ω for 200 rpm, whereas it shifts to 33 Ω at 1000 rpm. Thus it is a very important graph to explain the load characteristics of the machine. Between these speeds, the load, where the maximal point sits, increases smoothly. For instance, output power becomes 46 W, 106 W and 250 W at 300 rpm, 500 rpm and 1000 rpm, respectively.

The efficiency of the machine can be measured by considering the main losses at various speeds as in some earlier studies (Fig. 28(a,b)). However, it can also be measured directly by comparing the input and output power by a power analyzer, experimentally. While Fig. 28(a) shows the efficiency plots with respect to resistive loads, Fig. 28(b) presents the efficiencies with respect to rotor speed.

A Fluke type power analyzer is used for the experimental measurements. While the lowest efficiency has been found for 200 rpm, the maximal one has been measured for 1000 rpm. It is considered that the mechanical effects play important roles to limit the efficiency at lower speeds. The prototype machine reaches to 92.5% efficiency at the rated speed (i.e. 1000 rpm). Another reason for the efficiency loss is the airgap width. In order to minimize the mechanical frictions and protect the electrical units, a larger airgap has been used. It is expected that the efficiency will be increased further by assigning smaller airgap value. In that case, a better mechanical stabilization should be ascertained.

According to Fig. 28(b), the efficiency becomes maximal at 30 Ω beyond the speed of 800 rpm. However, it is worse for other loads. It has been also observed that higher loads such as 60 Ω may yield to higher efficiency values such as 85% as seen from the graph. Due to the mechanical instabilities in the setup, we could not try the higher speeds and we have left this issue to future studies.

Table 2 – Rated values of three phase AFPMG.

Rated power	250 W
Rated current	1.44 A
Rated voltage	58 V
Rated speed	1000 rpm
Efficiency	92.5%

In Table 2, the measured rated values of the proposed machine have been summarized. However, some optimization research can be realized just after a better mechanical processing, since the airgap optimization is important for these machines in order to achieve better efficiency and power density.

To conclude, the airgap of 1.5 mm should be tested for the cogging torque and generated energy density studies. We believe that the machine is promising to achieve good cogging torque value and efficiency.

Conclusions

A new three phase permanent magnet machine has been designed and implemented. The tests on the waveform patterns and theoretical findings prove that the new machine can generate 250 W at the rated speed. The optimized load for the rated speed has been found as 33 Ω and the efficiency gives the value of 92.5% according to the experimental measurements. Although the proposed machine has separated 12 cores with a special shape, its THD values are very well with good sinusoidal output. Frankly speaking, 0.4% THD value stands for loaded cases, whereas it increases up to 4.7% without electrical load.

The new generator is considered as a good candidate for wind turbine applications and it does not require any additional waveform improver, since it creates a sinusoidal output. The most important loss is found to be Copper loss and it can be decreased for high resistive loads substantially. Core losses have been found to be very low and promising for such a new machine.

Acknowledgments

The authors are grateful to Gazi University, Scientific Researches Project Unit for the support of this project under the Project Code: 07/2011-25 and European Union Ministry of Turkey, National Agency of Turkey for the support of this

project under the Project Code: 2015-1-TR01-KA203-021342 entitled *Innovative European Studies on Renewable Energy Systems*.

REFERENCES

[1] Sadeghierad M, Lesani H, Monsef H, Darabi A. Detail modeling of high speed axial flux PMG. Aust J Basic Appl Sci 2009;3(2):1467–75.

[2] Chan CC. Axial-field electrical machines-design and applications. IEEE Trans Energy Convers 1987;2(2):294–300.

[3] Guannan D, Haifeng W, Hui G, Guobiao G. Direct drive permanent magnet wind generator design and electromagnetic field finite element analysis. IEEE Trans Appl Supercond 2010;20(3):1883–7.

[4] Barave SP, Chowdhury BH. Optimal design of induction generators for space applications. IEEE Trans Aerosp Electron Sys 2009;45(3):1126–37.

[5] Kurt E, Aslan S, Demirtaş M. Cogging torque exploration of radially and angularly directed fluxes in a new PM generator with the multiple stators. In: 7th. Int. Conf. & Exh. ecological vehicles and renewable energies – EVER'12, Monaco; 2012. p. 1–8.

[6] Gör H, Kurt E. Comparison of cogging torques in two different axial flux permanent magnet generators. In: EWRES, the European workshop & conference on renewable energy systems; 2013 [Antalya, Turkey].

[7] Kurt E, Gör H. Electromagnetic design of a new axial flux generator. In: IEEE proc. electronics, computer and artifical intelligence (ECAI 2014), 6th international conference:39-42; 23–25 Oct 2014 [Bucharest, Romania].

[8] Gholomian S, Yousefi A. Power density comparison for three phase non-slotted double-sided AFPM motors. Aust J Basic Sci 2010;4(12):5497–955.

[9] Vansompel H, Sergeant P, Dupre L, Bossche AV. Axial-flux PM machines with variable air gap. Ind Electron IEEE Trans 2014;61(2):730–7.

[10] Garrison FP, Todd DB, Comanescu M, Muller BA. Design and testing of a permanent magnet axial flux wind power generator. In: 2008 IAJC-IJME international conference, Nashville; 2008. p. 190–202.

[11] Patterson D, Spee R. The design and development of an axial flux permanent magnet brushless DC motor for wheel drive in a solar powered vehicle. In: IEEE industrial applications society conf., Denver; 1994. 1,188–195.

[12] So-Young S, Jae-Hoon J, Yu-Seop P. Improved analytical modeling of axial flux machine with a double-sided permanent magnet rotor and slotless stator based on an analytical method. Magn IEEE Trans 2012;48(11):2945–8.

[13] Chalmers BJ, Wu W, Spooner E. An axial-flux permanent-magnet generator for a gearless wind energy system. IEEE Trans Energy Conver 1999;14(2):251–7.

[14] Aydin M, Guven MK. Design of several permanent magnet synchronous generators for high power traction applications. In: Electric machines & drives conference (IEMDC), Chicago; 2013. p. 81–7.

[15] Sadeghierad M, Lesani H, Monsef H, Darabi A. Design considerations of high speed axial flux permanent magnet generator with coreless stator. In: Power engineering conference, IPEC; 2007. p. 1097–102. Singapore.

[16] Duy NT, King-Jet T, Shao Z, Hoan Thong N. A novel axial flux permanent-magnet machine for flywheel energy storage system: design and analysis. IEEE Trans Ind Elect 2011;58(9):3784–94.

[17] Wang RJ, Kamper MJ. Calculation of eddy current loss in axial field permanent magnet machine with coreless stator. IEEE Trans EC 2004;19(3):532–8.

[18] Yicheng C, Pillay P, Khan A. PM wind generator comparison of different topologies. Ind Appl Conf 39th IAS Annu Meet 2004;3:1405–12.

[19] Bumby JR, Martin R. Axial-flux permanent-magnet air-cored generator for small-scale wind turbines. Proc IEE- Electr Power Appl 2006;152(5):63–73.

[20] Al-Aawar N, Hijazi TM, Arkadan AA. Design optimization of axial-flux permanent magnet generator. In: Electromagnetic field computation (CEFC), 14th biennial IEEE conference, Chicago; 2010. p. 1.

[21] Jian L, Da-Woon C, Yun-Hyun C. Development of a natural cooled axial flux permanent magnet generator for wind turbine. In: Industrial electronics (ISIE), IEEE international symposium, Hangzhou; 2012. p. 635–40.

[22] Kurt E, Gör H, Demirtaş M. Theoretical and experimental analyses of a single phase permanent magnet generator (PMG) with multiple cores having axial and radial directed fluxes. Energy Convers Manag 2014;77:163–72.

[23] Chan TF, Weimin W, Lai LL. Magnetic field in a transverse- and axial-flux permanent magnet synchronous generator from 3-D FEA. Magn IEEE Trans 2012;48(2):1055–8.

[24] Chan TF, Lai LL, Shuming X. Field computation for an axial flux permanent-magnet synchronous generator. Energy Convers IEEE Trans 2009;24(1):1–11. http://dx.doi.org/10.1109/TEC.2008.2011830.

[25] Don-Ha H, Ki-Chang L, Do-Hyun K, Yong-Joo K, Kyeong-Ho C, Doh-Young P. An modular-type axial-flux permanent magnet synchronous generator for gearless wind power systems. In: Industrial electronics society, IECON 2004. 30th annual conference of IEEE, 2; 2004. p. 1396–9.

[26] Gieras JF, Wang RJ, Kamper MJ. Axial flux permanent magnet brushless machines. 2nd ed. Springer; 2008.

[27] Wanjiku JG, Jagau H, Khan MA, Barendse PS. Minimization of cogging torque in a small axial-flux PMSG with a parallel-teeth stator. In: Energy conversion congress and exposition (ECCE). IEEE; 2011. p. 3687–93.

[28] Kurt E, Gör H. Exploration of losses in a new axial flux permanent magnet generator (AFPMG). In: The 3th international conference on information processing and electrical engineering (ICIPEE 14); 2014 [Tebessa, Algeria].

[29] Kurt E, Aslan S, Gör H, Demirtas M. Electromagnetic analyses of two axial-flux permanent magnet generators (PMGs). In: IEEE proc. powereng; 13–17 May 2013. p. 290–4 [Istanbul, Turkey].